Journal of Structural Geology 32 (2010) 1768–1782

Contents lists available at ScienceDirect

Journal of Structural Geology

journal homepage: www.elsevier.com/locate/jsg

Structural controls on leakage from a natural CO_2 geologic storage site: Central Utah, U.S.A.

Ben Dockrill [a,*], Zoe K. Shipton [b]

[a] Department of Geology, Trinity College Dublin, Dublin 2, Ireland.
[b] Department of Geographical and Earth Sciences, University of Glasgow, Glasgow G12 8QQ, Scotland

ARTICLE INFO

Article history:
Received 26 May 2009
Received in revised form
26 November 2009
Accepted 19 January 2010
Available online 28 January 2010

Keywords:
Fault zone
Damage zone
Fluid flow
Co_2
Hydrocarbons

ABSTRACT

Faults and associated fracture networks can significantly influence regional flow of groundwater, hydrocarbons and other fluids. The distribution of CO_2 springs and seeps along the Little Grand Wash fault and Salt Wash faults in central Utah is controlled by along-fault flow of CO_2-charged groundwater from shallow aquifers (<1 km deep). The same faults are the likely conduits that charge the shallow aquifers with CO_2 from depth. We document fault zone trace geometry and architecture, and evidence for palaeo-fluid flow within the footwalls of both faults. Evidence for palaeo-fluid flow consists of extensive bleaching of sandstones and some siltstones, mineralisation of carbonates and celestine veins and minor hydrocarbon staining. The field evidence shows that the pathways for multiple phases of fluid flow were structurally controlled utilising the fracture network developed in the damage zone of the faults. To investigate the likely effect of these faults on the regional fluid-migration pathways at depth, a 3D model of the faulted system was generated and a fault seal analysis applied to predict the cross-fault sealing capabilities of the studied faults. Due to the scarcity of subsurface data, the results are not conclusive but suggest probable multiple cross-fault leak points for fluids to migrate across the fault, in contrast to the field observations that indicate fault-parallel flow. This comparison of field observations to the modelling approach demonstrates the inability of conventional seal analysis techniques to predict fault-parallel fluid leakage and highlight the effects fracture networks in the damage zone, especially at structural complexities along the fault, have in producing pathways for vertical flow. Multiple fluids have utilised similar fault-parallel pathways over geological time demonstrating that such pathways have the potential to cause long-term leakage from hydrocarbon reservoirs and CO_2 storage sites.

1. Introduction

Faults and associated fracture networks can play a significant role in the subsurface migration of various fluids. Focussing of flow related to fault geometry has been demonstrated in geothermal fields (Curewitz and Karson, 1997; Rowland and Sibson, 2004), hydrothermal/epithermal systems (Breit and Meunier, 1990; Micklethwaite, 2009) and petroleum systems (Chan et al., 2000; Garden et al., 2001; Gartrell et al., 2004). In most studies, flow is concentrated in the fracture network (commonly referred to as the damage zone) that is developed around a main zone of slip. Complexities along a fault related to terminations and/or linkages between fault segments are commonly domains of high fracture density and connectivity and are therefore likely to focus flow (Curewitz and Karson, 1997; Anderson and Fairley, 2008; Eichhubl et al., 2009). Models that predict fault properties based on the throw and host rocks cut by the fault (Yielding et al., 1997; Yielding, 2002; Bretan et al., 2003) generally rely on oversimplified fault geometries and complexities, leading to the possibility of underestimating likely leakage points due to fault throw partitioning and simplified fault linkages (Childs et al., 1996, 1997), and do not account for along-fault flow.

This study investigates a natural leaking CO_2-rich system at the northern end of the Paradox Basin in central Utah, United States. In this locality, the Little Grand Wash fault and northern fault of the Salt Wash graben provide lateral barriers to present-day cross-fault flow, but provide pathways through the cap rock via damage zone fractures to allow CO_2 and additional fluid regimes to leak to the surface (Shipton et al., 2004, 2005). Multiple mineralisation and diagenetic products associated with past and present migration of fluids along both faults demonstrate structural controls influencing multiple fluid regimes to vertically migrate through a thick interbedded sandstone–shale stratigraphy. By combining outcrop

* Corresponding author. Present address: Chevron Australia, 250 St Georges Terrace, Perth, WA, Australia. Tel.: +61 8 9216 4141; fax: +61 8 9216 4103.
E-mail address: ben.dockrill@chevron.com (B. Dockrill).

0191-8141/$ – see front matter © 2010 Elsevier Ltd. All rights reserved.
doi:10.1016/j.jsg.2010.01.007

analysis of the fault zone and associated fluid-migration products with analysis of fault rock integrity through modelling, we have examined constraints on leakage from shallow reservoirs. Faults can form barriers to flow either by juxtaposing reservoir rock against low-permeability clay-rich non-reservoir rock to create a juxtaposition seal, or when processes of fault rock generation form a low-porosity and low-permeability fault rock. By analysing the fault rocks and the processes and factors that contribute to the failure of this system, we can identify and highlight the roles faults can play in trapping and transmitting fluids. These results demonstrate the impact fault zones can have on fault-parallel leakage from a robust structural trap and highlight the potential risks when assessing seal integrity for structural traps in the hydrocarbon and emerging CO_2 geologic storage industries.

2. Geological setting

The field area is located at the northern end of the Paradox Basin in the Colorado Plateau region of the United States (Fig. 1), a late Palaeozoic to Mesozoic intracratonic basin infilled with a thick sequence of evaporite, carbonate and clastic sediments (Hintze, 1993). The basin is defined by the areal extent of the Pennsylvanian Paradox Formation, which contains nearly 2 km of evaporates (Doelling et al., 1988). The basin has been investigated for hydrocarbons (Peterson, 1973, 1989; Hansley, 1995; Huntoon et al., 1999) and mineral resources (Breit and Meunier, 1990; Morrison and Parry, 1986). Multiple reservoirs have accumulated CO_2 for extended periods of times (Allis et al., 2001, 2005; Moore et al., 2005; Shipton et al., 2004, 2005; White et al., 2005). Some of these are now currently being exploited, predominantly for enhanced oil recovery (i.e. Bravo and McElmo domes – Allis et al., 2001). Other reservoirs leak CO_2 due to the influence of faults (Springerville-St Johns – Moore et al., 2005; Hurricane fault – Nelson et al., 2009) and/or boreholes (Woodside – Doelling, 1994).

The stratigraphy in the Paradox basin ranges from the Pennsylvanian Paradox Formation to the Mid Cretaceous Mancos Shale, though only the Upper Jurassic to Mid Cretaceous succession crops out in the field area (Fig. 1). The Pennsylvanian and Permian formations consist of marine carbonates and shales that are potential sources of the CO_2 (Heath et al., in press; Wilkinson et al., 2008) and hydrocarbons (Peterson, 1973, 1989; Huntoon et al., 1999; Chan et al., 2000; Garden et al., 2001). The aeolian reservoir sandstones of the Permian White Rim Sandstone are capped by fluvial and lacustrine shales of the Triassic Moenkopi and Chinle formations. The aeolian Lower Jurassic Wingate and Navajo sandstones are important regional aquifers separated by the fluvial Kayenta Formation aquitard. Forming a seal above the Navajo Sandstone is the Mid-Jurassic Carmel Formation, a complex sabkha sequence of sandstone, siltstone, mudstone, limestone, anhydrite and gypsum. The youngest reservoir units in the basin are the Mid-Jurassic Entrada and Curtis aeolian to marginal marine sandstones, overlain by marine siltstones and shales of the Middle Jurassic Summerville Formation. The remaining stratigraphic sequence is dominated by shales with small, disconnected reservoir units. The Upper Jurassic Morrison Formation consists of stacked fluvial sandstone channels, interspersed and overlain by lacustrine shales. The lower Cretaceous Cedar Mountain Formation lacustrine shales are overlain by conglomeritic fluvial channels from the lower Cretaceous Dakota Formation. The youngest rocks exposed in the field area are marine marls of the Middle Cretaceous Mancos Shale.

The shallowly north- to northwest-plunging, open Green River anticline is one of a series of northwest-trending folds that have growth histories related to salt movement in the Paradox Formation since the Permian (Doelling et al., 1988). The Green River anticline is cut by the Little Grand Wash fault and the Salt Wash graben. Timing of movement along both faults is poorly constrained, with the youngest faulted stratigraphy being the Mid Cretaceous Mancos Shale, though evidence presented by Pevear

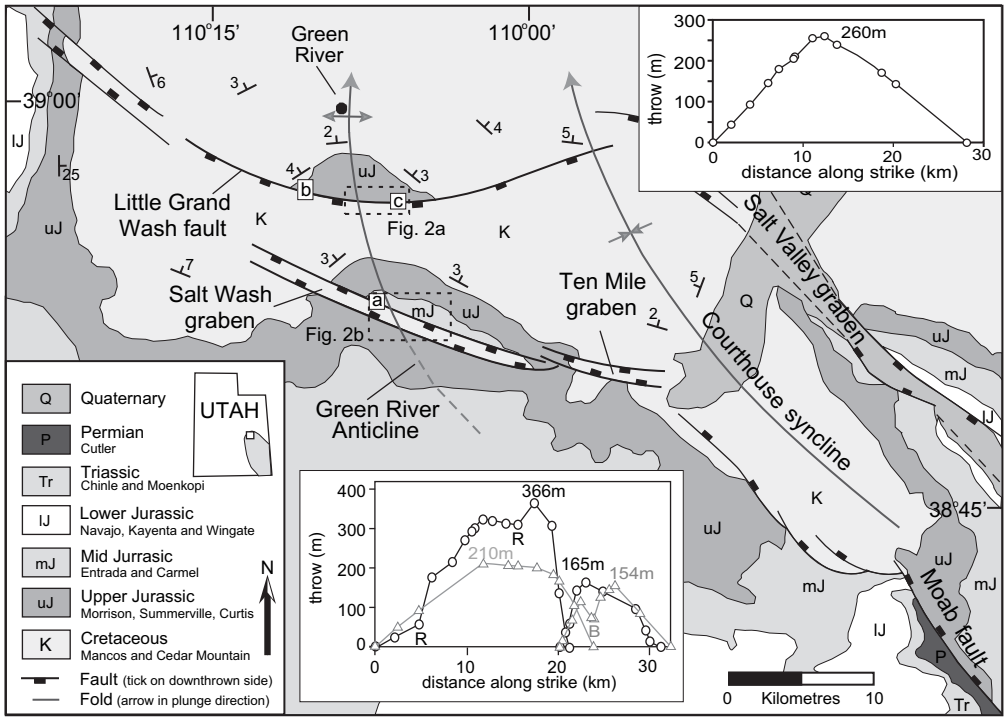

Fig. 1. Geological map of the study area in central Utah, USA. Structural data from field work and McKnight (1940) and Doelling (2001, 2002). Dashed boxes show the positions of Fig. 2. The letters a, b, c indicate position of the fault zone strip maps displayed in Fig. 3. Top right inset, throw distribution along the Little Grand Wash fault zone. Centre inset, throw distribution along the northern (black circles) and southern (grey triangles) Salt Wash graben. Note that relay ramps along the Salt Wash graben are coincident with throw minima.

et al. (1997) and Shipton et al. (2004) suggest possible early Tertiary to Quaternary movement. Where the fold axis of the Green River anticline is cut by the faults, CO_2-charged groundwater effuses from a series of geysers and springs (Doelling, 1994; Shipton et al., 2004, 2005). A series of actively-forming spring deposits and remains of ancient travertine deposits are found along or immediately to the North (i.e. in the footwall) of both fault systems (Fig. 2). All of the springs originate in the footwall though some of the travertine deposits drape over the fault into the hanging-wall. Additional CO_2-charged geysers occur where hydrocarbon or water boreholes have penetrated the footwall reservoirs, though some boreholes that penetrate the footwall reservoirs at depth do not leak (Shipton et al., 2005).

The faulting of the Green River anticline has created a series of stacked three-way anticlinal closures in the footwall reservoirs of the Little Grand Wash fault and northern fault of the Salt Wash graben. Southeast-directed regional groundwater flow (Hood and Patterson, 1984) suggests that CO_2-charged meteoric fluids have been focussed up the north-plunging Green River anticline towards the central sections of the faults. Carrier beds for the CO_2-charged water include the Lower Jurassic Wingate and Navajo sandstones and the Mid-Jurassic Entrada and Curtis sandstones (see Heath et al., in press). The cap rocks for these structural closures are provided by clay-rich and evaporitic beds in the sequence, while lateral barriers to flow are provided by the faults (Shipton et al., 2004, 2005). Stable isotope data indicate that travertine deposits along both faults have resulted from a common CO_2-rich fluid (Shipton et al., 2005; Dockrill et al. in prep). Furthermore, leakage is confined to the footwall of both faults with no isotopically similar carbonates located elsewhere in the area. The distribution of springs and travertines therefore suggests that the studied faults are providing a long-lived pathway for a significant proportion of CO_2-rich fluids to migrate vertically through multiple cap rocks in the footwalls of both faults.

3. Fault geometry

The east–west trending south-dipping Little Grand Wash fault juxtaposes late Jurassic and Cretaceous siliciclastics at the surface (Fig. 1). The fault has a 30 km long, arcuate surface trace that splits into two dominant fault strands in the central part of the structure, extending from 3.2 km east to 0.1 km west of the Green River (Fig. 2). The two sub-parallel fault strands introduce structural complexities to the fault with a series of prominent fault bends, branch points and relay ramps. Between and surrounding the two main strands, a complicated array of minor faults and relays has

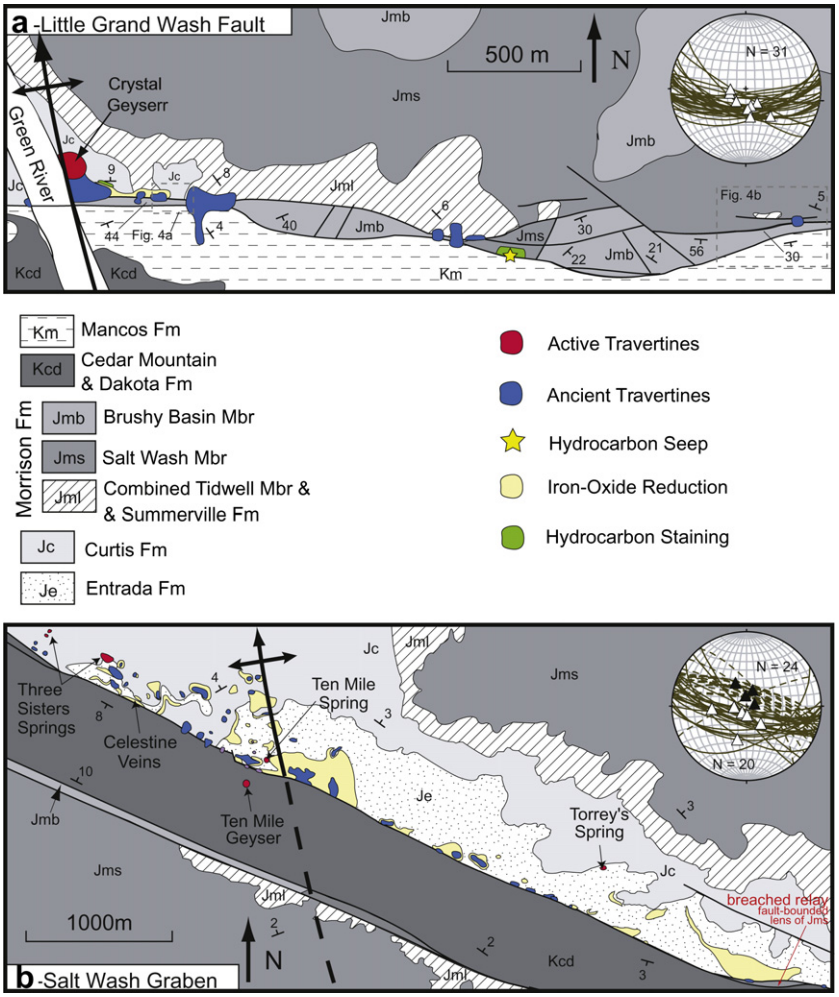

Fig. 2. Relationship between Little Grand Wash fault and Salt Wash graben structures and locations of CO_2 leakage (modern and ancient travertines) and evidence for past fluid flow. (a) Central part of the Little Grand Wash fault where it splits into two main strands and cuts the hinge of the Green River anticline. Dashed boxes show the two locations for the fracture analysis in Fig. 4. (b) Detailed structure of the Salt Wash graben. Equal angle stereonets show strike and dip of faults with lineations (triangles) indicating direction of fault movement. N is the number of faults measured. Closed triangles correspond to northern fault lineations, while open triangles indicate southern fault lineations. (For interpretation of the references to colour in this figure legend, the reader is referred to the web version of this article).

created multiple structural terraces with varying dips (Fig. 2; see also Fig. 7 in Vrolijk et al., 2005). Away from the central zone, a single fault strand is present. In the subsurface, the down-dip extent and geometry of the fault is uncertain, though drilling records for two exploration wells (Amerada Hess 1 and 2) that intersect the fault at depth suggest that the fault may offset rocks as old as Pennsylvanian in age.

The dip of the main fault strands along the Little Grand Wash fault varies but is generally steep, averaging 70° to the south. Slip indicators show that the fault is mostly dip-slip with some local oblique right- and left-lateral movement in the structural terraces (stereonets in Fig. 2). The maximum stratigraphic offset across the fault is 260 m immediately east of the Green River with throw systematically decreasing towards the exposed surface fault tips (Fig. 1).

The Salt Wash graben forms part of a 31 km-long structure consisting of two west-northwest-trending grabens (Salt Wash and Ten Mile grabens) linked by a left-stepping relay ramp (Fig. 1). Both grabens are bound by sub-parallel, inward-dipping normal faults that overlap for a kilometre and result in a steep, east-dipping ramp connecting the northern and southern footwalls between the two down-dropped structures (Williams, 2005). At the surface the graben juxtaposes Mid-Jurassic and Cretaceous siliciclastics. The faults' subsurface geometry and vertical penetration is unknown due to the lack of subsurface data. However, reservoir-scale faults to the SE (Moab fault and Salt Valley graben; Fig. 1) commonly penetrate the Pennsylvanian Paradox Formation in the immediate region (Doelling et al., 1988; Foxford et al., 1998). Further discussion will be limited to the Salt Wash graben as the Ten Mile graben is off structural trend in relation to the Green River anticline and associated fluid-flow features, and field mapping shows no evidence for present or past fluid flow along the Ten Mile graben (Williams, 2005).

The Salt Wash graben is 20 km long, with an average width of 800 m. Bed dips within the graben range from sub-horizontal in the centre of the graben to up to 25° towards the bounding faults. The northern fault is a single strand that dips steeply to the south, averaging 73° (Fig. 2). Sporadic geometric complexities are encountered along the fault trace in the form of relay ramps and branch points. The southern fault dips steeply to the north, averaging 75° and displays rare relay ramps and branch points along strike. To the east, the southern fault bends eastward, truncating the northern fault and terminating against the southern fault of the Ten Mile graben. Rare slickensides indicate predominantly dip-slip movement. The maximum stratigraphic offset across the northern fault is 366 m and across the southern fault is 210 m (Fig. 1). Variation in throw along strike of both faults defines a throw profile consistent with a kinematically linked fault system (e.g. Dawers and Anders, 1995).

4. Fault architecture

At the surface, both faults displace an interbedded sequence of sandstones and shales. The surface exposures of both fault zones contain a fault core, where most of the slip is accommodated, surrounded by a damage zone of smaller-offset structures (c.f. Caine et al., 1996). The fault cores are typically 1–3 m wide and contain three principal deformation elements: (1) clay-rich gouge; (2) entrained sections of host rock; and (3) slip zones (Fig. 3; Fig. 9 in Vrolijk et al., 2005). The gouge forms centimetre- to metre-thick zones with a highly foliated, fault-parallel fabric that locally forms an S–C fabric adjacent to slip zones. X-ray diffraction analyses show that the gouge is composed of quartz and clay minerals including illite, illite–smectite and kaolinite, with sporadic halite, calcite, feldspar and haematite. Entrained sections of sand-rich host rock include fractured, elongated lenses of sandstone and siltstone, 2–20 cm thick, and coherent but highly-fractured slabs up to 1 m thick with occasional deformation bands and rare calcite veining. These lenses and slabs are most evident where Mid to Late Jurassic sandstones are located in the footwall. The isolated lenses are enveloped by gouge and have long axes orientated sub-parallel to the gouge foliation. The striated and intensely foliated clay-rich slip zones are 5–100 mm thick with highly polished striated surfaces, and occasionally contain angular, sand-rich, pebble-sized clasts. Slip zones define the limit of the fault core, separating fault rock from fractured host rock. Slip zones are also common inside the fault core, where they separate fault gouge and sandstone pods derived from different lithologies. These observations suggest that the slip zones accommodate the majority of the slip within the fault core.

Variations in fracture orientation and density in the damage zone were characterised along transects in two relatively well-

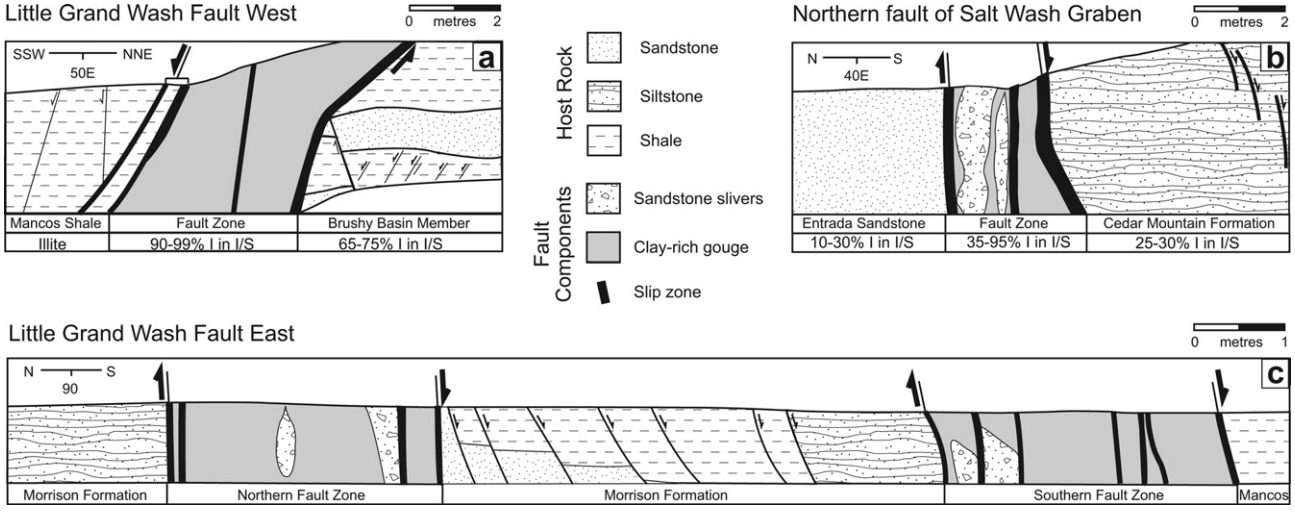

Fig. 3. Structural transects across the fault core at (a) the Little Grand Wash fault western outcrop, (b) the northern fault of the Salt Wash graben and (c) the Little Grand Wash fault eastern outcrop. The location of transects are shown in Fig. 1. Transects are at a 1:1 scale with respective scale bars in top right corners. Exposures were cleaned with trowels and brushes to remove the top weathered rind of the clay-rich rocks. Mineralogy of fault core gouge was assessed using X-ray diffraction. I in I/S refers to illite in illite/smectite mixed layers.

exposed areas along the Little Grand Wash fault (Fig. 4). The Little Grand Wash fault damage zone is dominated by a broadly east–west trending set of fractures that locally reflect the strike of the fault (Fig. 4). Immediately adjacent to the fault core a network of shear fractures and joints broadly diminishes in frequency outward into the host rock. Where observed, there is little to no displacement associated with the fractures and they are occasionally infilled with carbonates or sulphates. Variations from this trend are observed in a relay ramp between two fault strands (scanline 4) and in the hanging-wall shales (scanline 7). The relay ramp contains a diverse array of fracture orientations that are likely due to complicated three-dimensional strain during the development of the ramp. Distinct northwest-trending fractures at the top of the ramp (scanline 3; Fig. 4a) are likely the result of rotation and steepening of strata into the fault zone. The varied fracture orientations in the hanging-wall shales (scanline 7; Fig. 4b) may represent pre-existing fractures overprinted by later fault-associated fractures, or differing strain accommodation in the clay-rich strata compared to the sand-rich footwall strata.

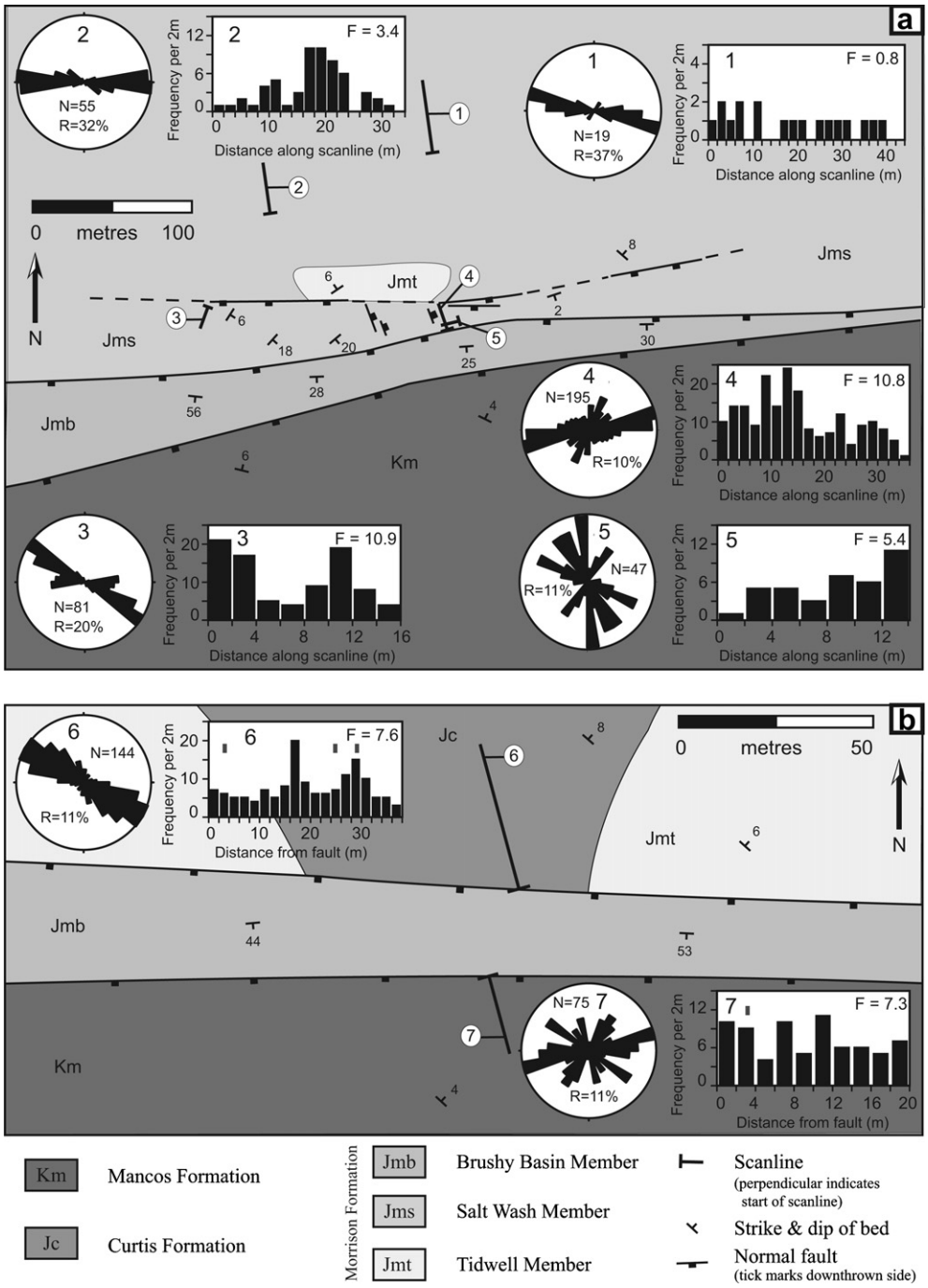

Fig. 4. Fracture analyses along the Little Grand Wash fault. (a) Five scanlines within and away from a partially breached footwall relay ramp along the northern of two main fault strands with a combined throw of 245 m. (b) Two scanlines near two closely-spaced fault strands with a combined throw of 255 m. To limit bias due to transect orientation (Park and West, 2002) where possible the scanlines were orientated perpendicular to the master fault. Fracture orientation (rose diagrams, R = % of fractures in largest petal) and frequency (histograms, 2 m bins, F = mean number of fractures per 2 m bin) are shown for each scanline.

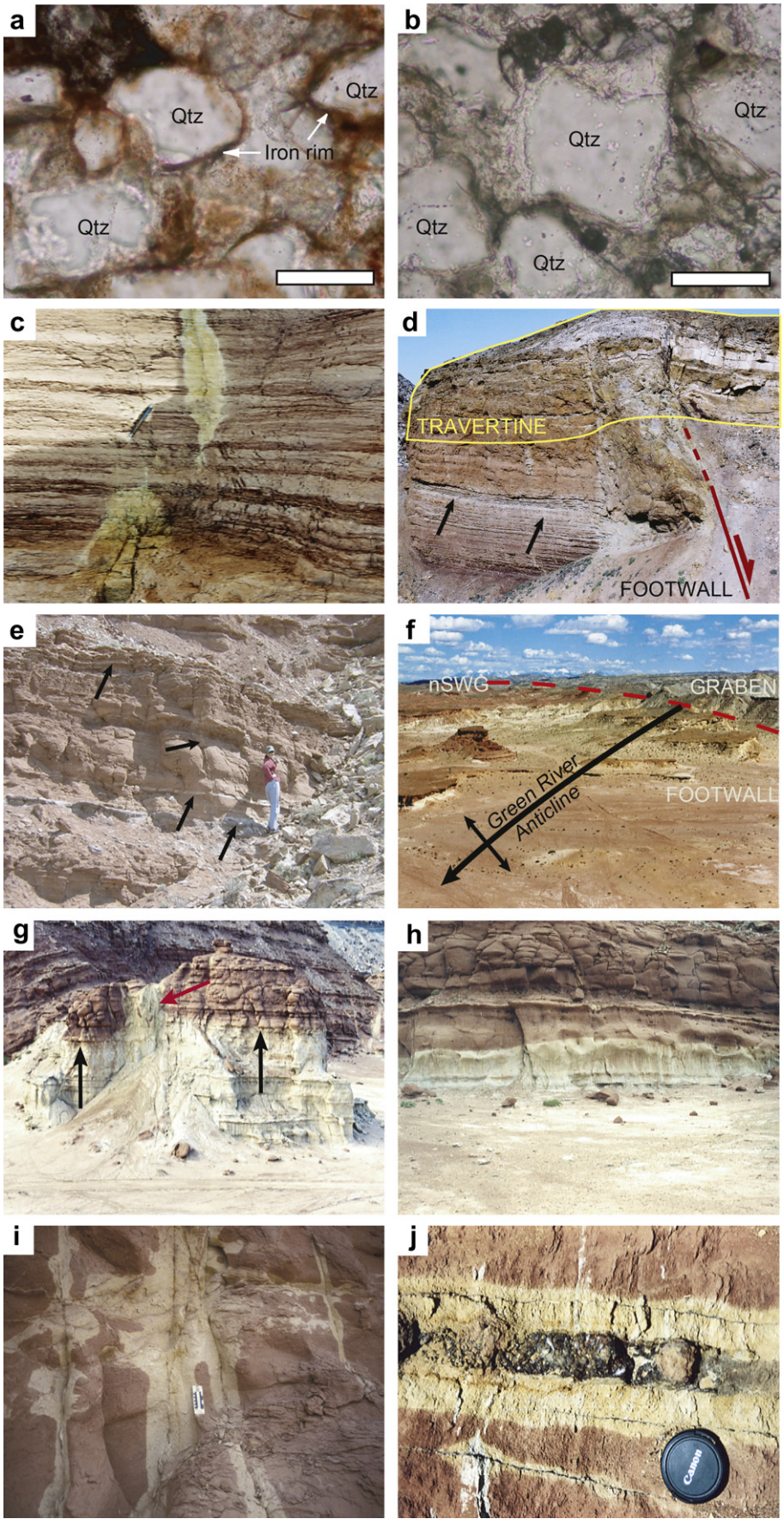
a
Qtz
Qtz
Iron rim
Qtz
b
Qtz
Qtz
Qtz
Qtz
c
d
TRAVERTINE
FOOTWALL
e
f
nSWG
GRABEN
Green River
Anticline
FOOTWALL
g
h
i
j

5. Evidence for fluid flow and leakage

At present, CO_2-charged groundwater is emanating from springs and geysers along both faults and an active hydrocarbon seep is located in the immediate footwall of the Little Grand Wash fault. Additionally, the soil gas surveys of Allis et al. (2005) show that focussed areas of high CO_2 flux occurs along the faults, not all of which are associated with effusion of CO_2-charged groundwater. At the surface, the CO_2-charged groundwater precipitates travertine mounds. The positions of past CO_2 leak points are marked by partial to complete remnants of ancient travertine mounds (Shipton et al., 2005; Dockrill, 2006). Active and ancient travertine deposits are concentrated in the footwall of both faults proximal to where the Green River anticline axis is cut by the faults (Fig. 2). Stable isotope studies indicate that the ancient travertines were precipitated by the same CO_2-rich fluids that are currently leaking (Dockrill, 2006; Dockrill et al. in prep.). The ancient travertine deposits form resistant caps on top of numerous buttes (Fig. 5d) and are topographically higher than the actively-forming travertines (5f).

There are variations in the distribution and development of the travertine deposits between the two faults. The Little Grand Wash fault contains a series of discrete, well-developed, thick (1–10 m) deposits that are located in various footwall lithologies from the sand-rich Curtis Formation to clay-rich sections of the Morrison Formation (Fig. 2a). The deposits form in the immediate footwall but can drape over the fault into the hanging-wall. Additionally, the deposits are confined to sections where the two main fault strands are close together and/or there are pronounced structural complexities such as fault bends and relay ramps. The northern fault of the Salt Wash graben contains mainly thinner (0.5–4 m) and less well-developed deposits compared to the Little Grand Wash fault. They are located in the sand-rich Entrada and Curtis formations with deposits predominantly confined to the immediate footwall, occasionally draping into the adjacent graben. However, around the Green River fold axis deposits increase in number and extend further into the footwall (Fig. 2b). The easternmost travertine deposits along this fault are associated with a breached relay ramp.

Bleaching of sandstones occurs to varying degrees in the footwalls of both faults, and is spatially associated with the travertine deposits. The bleaching is characterised as the loss of haematite rims mainly around sand grains (Fig. 5 a and b) resulting in a colour change in the footwall sandstones from ubiquitous red of the unbleached rock to yellow/white. The minor proportions of siltstones affected by bleaching also show a transition to paler colours. The distribution of bleaching in the footwalls of both faults is focussed in the faulted fold axis of the Green River anticline, though its spatial extent varies depending on the footwall lithologies. Along the more shale-rich Little Grand Wash fault footwall, bleaching is mainly confined to the base of ancient travertine deposits (Fig. 5c) or limited sections of the sand-rich Curtis Formation (Fig. 5d). At the base of the ancient travertines, bleaching is characterised by thin haloes (1–20 cm wide) around sub-vertical fractures, commonly infilled with aragonite or calcite veins and sub-horizontal tabular bleached bodies (5–200 cm thick) that extend laterally as dendritic stringers up to 200 m from the fault. The thickness of the bleached haloes and tabular bodies is dependant on the lithology; with clay-rich, lower porosity units (i.e. Morrison Formation) having thinner bleached zones relative to the sand-rich, higher porosity units (i.e. Curtis Formation). Bleaching away from the travertines is constrained to lower sections of the Curtis Formation, with the bottom 2 m of the outcropping sandstone partially to completely bleached, while the next 4m contains sporadic, thin bleached horizons (1–10 cm thick) sub-parallel to bedding and thin bleached haloes (1–5 cm thick) surrounding steeply-dipping fractures that are sporadically infilled with calcite or rare gypsum veins. Above this, bleaching is rare within the Curtis Formation and the overlying more clay-rich lithologies away from the travertines. Celestine and calcite veins are found associated with the bleaching (Fig. 5j).

Along the more sand-rich rocks exposed in the footwall of the northern fault of the Salt Wash graben, the red Entrada sandstones are extensively bleached to pale yellow (Fig. 5e). In the lower section of the exposed Entrada Formation (up to 8 m thick), sandstones are completely bleached, and the contact between bleached and unbleached sandstone does not follow bedding contacts (Fig. 5f and g). Above this contact, bleaching is mainly located around clusters of steeply-dipping fractures with bleached haloes up to 5 m wide (Fig. 5h). Pervasive reduction of the lower parts of the Entrada and Curtis sandstones extends up to 300 m into the footwall (Fig. 2). Beyond this region, bleached sandstones are only observed at the base of ancient travertine deposits and around steeply-dipping fractures. Similar to the Little Grand Wash fault, bleaching at the base of travertine deposits is characterised mainly by reduction haloes (up to 50 cm wide) around fractures, sometimes infilled with calcite, aragonite or gypsum (Fig. 5i) and limited sub-horizontal tabular reduction bodies (up to 2 m thick). Additional bleaching is also observed around steeply-dipping fracture clusters up to 400 m into the footwall. Close to the fault, a significant proportion of the fractures within the Entrada and Curtis sandstones are accompanied by reduction haloes, 5–200 cm wide. Further into the footwall, sporadic clusters of fractures, generally oblique to the fault, contain thinner reduction haloes (1–100 cm wide) that continue for as far as the Curtis sandstone crops out at the surface. Away from the anticline axis, the only significant patch of bleaching occurs by the breached relay where the easternmost ancient travertine is found (Fig. 2).

Hydrocarbon staining is limited to sandstones of the Curtis Formation (Fig. 6a) and the Salt Wash Member of the Morrison Formation close to or between the main fault strands of the Little Grand Wash fault. Hydrocarbon-stained sandstones are identified by a greyish colour, a musty petroleum odour when freshly broken and the occasional presence of bitumen veins. Hydrocarbon staining in the Curtis Formation is rare and limited to the same stratigraphic section that contains the bleaching, with 5–20 cm thick horizons of grey sandstone bordered by 1–5 cm thick, yellow to white bleached haloes (Fig. 6b). Conversely, hydrocarbon staining in the Salt Wash Member is more abundant with a 10 m thick sequence of stained beds between the two main fault strands. The stained sandstones are dark grey to white, are inundated with

Fig. 5. Iron-oxide reduction in the footwall of the Little Grand Wash fault and northern fault of the Salt Wash graben. Photomicrographs of Curtis Sandstone with (a) quartz (Qtz) grains rimmed by haematite and (b) haematite rims removed from quartz grains. (c) Reduction haloes surrounding sub-vertical fractures in the Curtis Formation (pen is 15 cm long). (d) Tabular reduction bodies (black arrows) extending into the Curtis Formation footwall. Yellow outline shows extent of overlying travertine deposit; dashed line is the fault trace. (e) Sporadic reduction horizons in the Curtis formation in the footwall of the LGWF. (f) View of the reduced, yellow Entrada sandstones in the core of the Green River anticline facing east. Away from the anticline, sandstones revert back to a red colour. Trace of the fault (nSWG) marked with a dashed line. (g) Entrada sandstone butte with lower half completely reduced and upper half only reduced around a fracture cluster (red arrow). Note reduction is not bed confined with a varying upper contact (cf. black arrows). Height of butte approximately 18 m. (h) Undulating reduction front in Entrada sandstone demonstrating that the colour change is not depositionally controlled. (i) Reduction haloes surrounding fractures in Entrada sandstone at the base of a travertine deposit (scale card is 16 cm long). (j) Celestine vein with reduction halo (lens cap 8 cm in diameter). (For interpretation of the references to colour in this figure legend, the reader is referred to the web version of this article.)

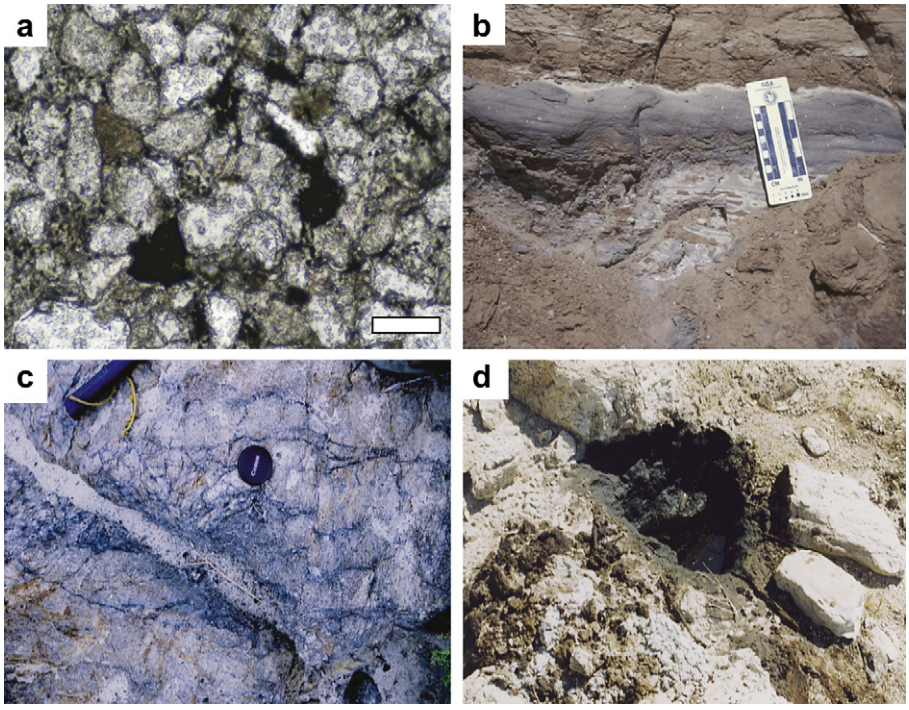

Fig. 6. Hydrocarbon staining along the Little Grand Wash fault. (a) Spherical oil globules interspersed around grains and within the matrix of the Curtis sandstone. Scale bar is 1 mm. (b) Hydrocarbon-stained Curtis sandstone with a thin white reduction halo (scale card is 16 cm long). (c) Fractures with a distinct hydrocarbon stain (lens cap is 8 cm in diameter). (d) Fresh oil seep at the base of the hydrocarbon-saturated Salt Wash sandstones. The width of the shallow pit is approximately 20 cm.

bitumen veins and contain many sub-vertical fractures with a hydrocarbon coating (Fig. 6c). At the base of this sequence, a hydrocarbon seep has been active since at least the beginning of the 20th century (Lupton, 1914; Fig. 6d).

6. Fault modelling

To place the fault-parallel fluid-migration observed in the field in context with potential for across-fault flow at depth, we need to predict the likely fault rocks and their fluid-flow properties at depth. A simple three-dimensional model of the northern Paradox basin area was generated using Midland Valley Exploration's 2Dmove and 3Dmove software tools. 2D and 3DMove are structural modelling software that uses geo-constrained data to build validated, balanced cross sections and surfaces, respectively. The model was constructed from approximately 200 hydrocarbon and water wells and 22 wire-line logs (Fig. 7a), and published (McKnight, 1940; Williams, 1964; Condon, 1997; Doelling, 2001, 2002) and new field data. These data were combined in 2DMove to generate a series of isopach and structure maps (Fig. 7b) that were used as templates to create 115 cross sections (e.g. Fig. 7c) covering the study area. The sections were subsequently connected by linear interpolation in 3DMove to create surfaces representing either faults or stratigraphic tops (Fig. 7d). The resulting 3D model consisted of 10 stratigraphic horizons representing the tops of units from the White Rim Sandstone to the Cedar Mountain Formation, based on major lithological changes and local formation divisions. The horizons are juxtaposed by 5 fault surfaces representing the Little Grand Wash fault and the bounding faults of the Salt Wash and Ten Mile grabens. Due to the lack of subsurface data penetrating or adjacent to the faults, they were modelled as single planar surfaces with constant dip. The three-dimensional model was validated in 2Dmove through section balancing during the 2D section and 3D surface construction (i.e. Midland Valley, 2004) and constrained by surface geologic data. The detailed methodology of the model construction can be found in Dockrill (2006).

To assess the likely sealing properties of the fault rocks at depth we undertook a simplified fault seal analysis in Traptester software, provided by Badley Geoscience. Regions of cross-fault reservoir–reservoir contact (potential cross-fault leak points) were identified from juxtaposition of footwall and hanging-wall cutoffs of key subsurface reservoirs against each fault using Allan diagrams (Fig. 8). To indicate the potential for membrane seal development by argillaceous smear or entrainment, Shale Gouge Ratio (SGR) calculations were applied to reservoir–reservoir contacts. SGR is the predicted percentage % shale within the fault (gouge assuming uniform mixing), calculated from the ratio of total shale bed thickness and fault throw (Yielding et al., 1997). SGR was the preferred smear algorithm used as it incorporates the effects of argillaceous material distributed through all siliciclastic units as opposed to individual argillaceous beds (cf. Clay Smear Potential and Shale Smear Factor; Yielding et al., 1997; Yielding, 2002) and it is the most commonly published algorithm with the best defined threshold sealing values (Yielding et al., 1997; Foxford et al., 1998; Sperrevik et al., 2000; Bretan et al., 2003; Gibson and Bentham, 2003). To establish the SGR along the fault, the V_{shale} content (volumetric shale content) of the modelled stratigraphy was estimated from representative wire-line gamma logs spliced together from wells proximal to the fault. The base shale and sand measurements were normalised to the 100% and 0% shale value respectively and a V_{shale} cutoff of 0.5 was used to define shale beds (Fig. 7e). Without calibrating wire-line logs against core data there is a risk of misinterpretation of argillaceous content; gamma logs, in particular, are poor detectors of kaolin and mica (Bretan et al., 2003). X-ray diffraction analyses of fault gouge from both faults (Fig. 3) indicate that illite and illite–smectite assemblages are the dominant clay minerals with minor amounts of kaolinite and no mica. The error related to using only gamma logs to determine V_{shale} is therefore probably small for this study. However, without

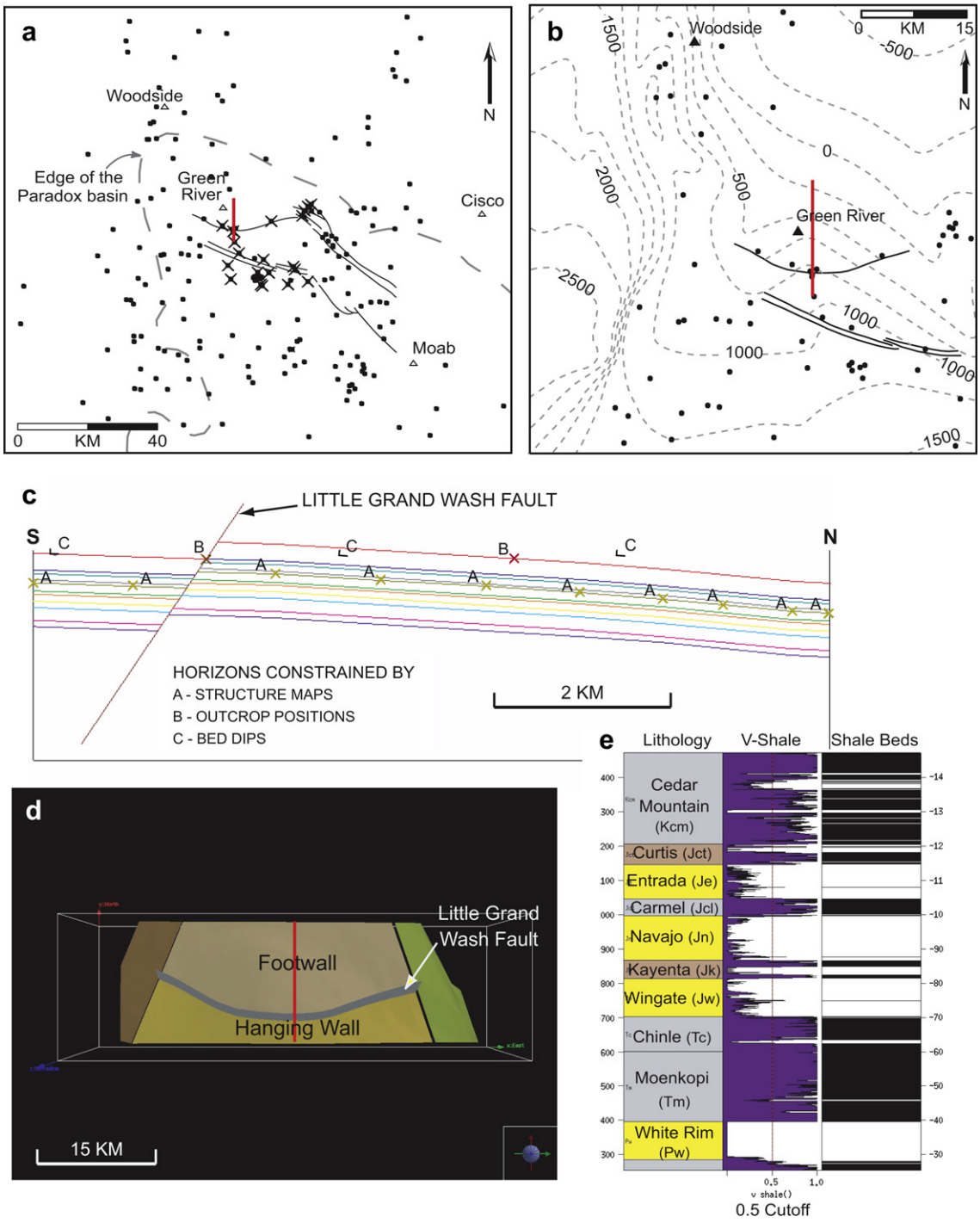

Fig. 7. Stages in the construction of the three-dimensional model used for fault seal analysis. The red line indicates position of the representative cross section display in Fig. 7. (a) Distribution of exploration well (circles) and wire-line log (crosses) data used to construct the model. (b) Structure contour map of the Navajo Sandstone created from a combination of well, field and published (McKnight, 1940; Doelling, 2001) data. (c) Representative cross section across the Little Grand Wash fault constructed in 2DMove from structure contour and isopach maps. (d) Generation of a three-dimensional surface in 3DMove from a series of cross sections. (e) Representative V_{shale} curve used in the model to define the shale content of the stratigraphic sequence. (For interpretation of the references to colour in this figure legend, the reader is referred to the web version of this article.)

direct calibration with core data uncertainty remains, and predicted fault rock values that are close to the threshold value for a continuous clay-rich fault gouge should treated with caution while higher values are considered more robust.

Potential carrier beds for the multiple fluid regimes in the subsurface include the Navajo, Wingate and White Rim sandstones. An Allan diagram of the Little Grand Wash fault shows that apart from self-juxtaposition towards fault tips, the Navajo Sandstone is juxtaposed against the Entrada Sandstone and the Wingate Sandstone is juxtaposed against sections of the Entrada and Navajo sandstones (Fig. 8a). Conversely, the White Rim Sandstone contains a good juxtaposition seal against the shale-rich Chinle and Moenkopi formations. The northern fault of the Salt Wash graben has the Navajo Sandstone juxtaposed against the Entrada Sandstone, the Wingate Sandstone juxtaposed against the Entrada and Navajo sandstones and the upper section of the White Rim Sandstone

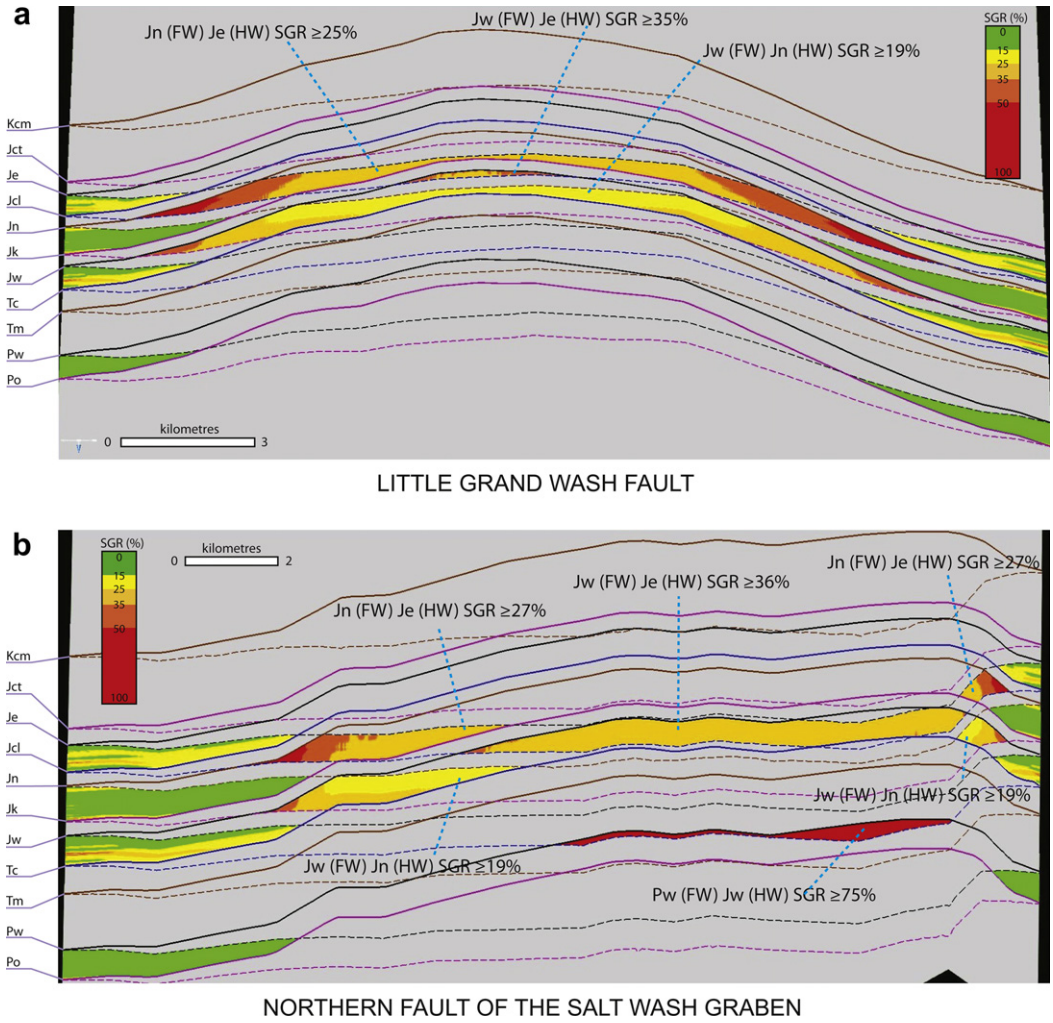

Fig. 8. Allan diagrams (Allan, 1989) of (a) the Little Grand Wash fault and (b) the northern fault of the Salt Wash graben. Coloured zones indicate SGR values at reservoir–reservoir juxtapositions. Solid and dashed lines indicate footwall and hanging-wall intersections along both faults, respectively. Key reservoir–reservoir juxtapositions and their minimum SGR values in the central sections of both faults are annotated for reference. Vertical exaggeration × 6. (For interpretation of the references to colour in this figure legend, the reader is referred to the web version of this article.)

juxtaposed against the Wingate Sandstone (Fig. 8b). These juxtapositions provide potential pathways for cross-fault flow if no membrane seal is developed in the fault rocks.

Calculated SGR values at reservoir–reservoir juxtapositions identified along both faults indicate values as low as 25% for the Navajo Sandstone, 19% for the Wingate Sandstone and 75% for the White Rim Sandstone. Outcrop (Foxford et al., 1998) and experimental (Sperrevik et al., 2000) studies suggest continuous argillaceous smears can develop from SGR values greater than ca. 20% and published studies of proven hydrocarbon fault traps indicate SGR between 15 and 25% generally represent the threshold for a leak–seal transition (Yielding et al., 1997; Yielding, 2002; Gibson and Bentham, 2003). However, without calibration of the SGR to analogues or nearby proven fault traps, the SGR threshold value for the fault to seal remains unknown and the development of a continuous argillaceous membrane seal that can maintain a fluid column is questionable. For this study, if a SGR value of 20% is used as a threshold between a fault sealing and leaking, there is potential for both faults to have cross-fault leak points in the footwall where the Wingate Sandstone is juxtaposed against the Navajo Sandstone and towards the fault tips where reservoirs are self-juxtaposed. Thus, depending on where fluids are sourced and their migration pathways, both faults possibly provide opportunities for cross-fault flow where development of a continuous argillaceous smear is questionable due to low SGR values.

Sensitivity analyses of the fault seal model were also undertaken using juxtaposition/triangle diagrams constructed in Traptester to 1) assess uncertainties related to the modelling of the faults from a sparse data set, and 2) assess the impact of using alternative smearing algorithms to calculate membrane seal potential. Fault modelling uncertainties relate to constraints imposed by a lack of subsurface data resulting in faults being modelled with constant vertical throw and as single fault planes with no geometrical complexity. The impact of changing the vertical throw profile along both faults can be examined by determining the maximum vertical change in throw of the modelled stratigraphic sequence calculated by using an aspect ratio (fault strike length/fault dip length) of 2.15 (Nicol et al., 1996). Fig. 9a shows the maximum change in throw will be ±15 m for the Little Grand Wash fault and ±20 m for the northern fault of the Salt Wash graben and that these changes will have minimal impact in juxtaposition relationships or SGR values. Of greater concern is not being able to replicate the outcrop expressions of the studied faults, with structural complexities observed in the field such as multiple fault strands and relay ramps having the potential to dramatically change throw profiles and reservoir juxtaposition relationships. The effect of multiple fault

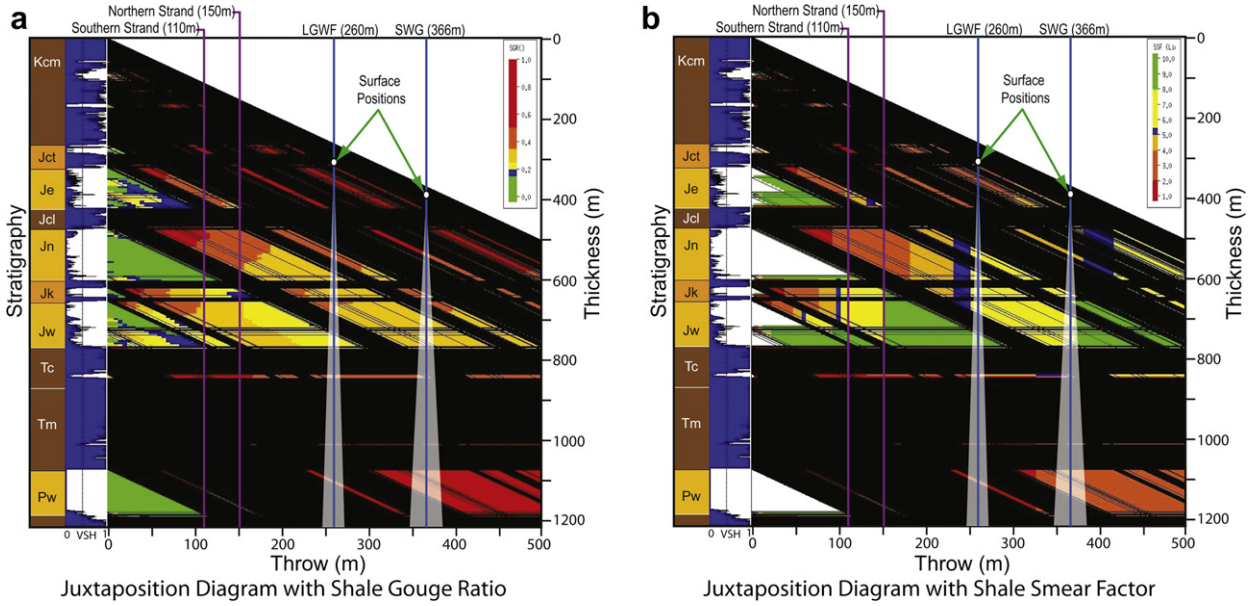

Fig. 9. Juxtaposition diagrams (Knipe, 1997) exploring uncertainties related to the fault seal model. Black areas on the juxtaposition diagrams represent reservoir or seal juxtaposed against seal and coloured areas indicate (a) shale gouge ratio and (b) shale smear factor values at reservoir–reservoir juxtapositions. Seals are defined as stratigraphy with V_{shale} (VSH) values greater than 0.5. Vertical blue lines represent the modelled maximum throw on the Little Grand Wash fault (LGWF) and northern fault of the Salt Wash graben (SWG). Vertical purple lines represent maximum surface throw on the Little Grand Wash fault partitioned between two fault strands. White shaded areas indicate maximum changes in down-dip throw along both faults. (For interpretation of the references to colour in this figure legend, the reader is referred to the web version of this article.)

strands is evident at the centre of the Little Grand Wash fault, where the total throw (260 m) is partitioned between the northern (150 m) and southern (110 m) fault strands (Fig. 9a). Compared to the single fault modelled in the seal analysis, throw partitioning between the two fault strands creates more areas of reservoir–reservoir juxtaposition and a general decrease in SGR values, making the faulted system more exposed to cross-fault flow. Relay ramps can also compromise the sealing capability of a fault through also partitioning throw between hard-linked fault strands as well as providing direct leakage pathways out of structural closures between soft-linked faults (Hesthammer and Fossen, 2000; Rotevatn et al., 2007). The along strike outcrop expression of the Little Grand Wash fault shows multiple examples of hard- and soft-fault linkage and throw partitioning between multiple fault strands. The northern fault of the Salt Wash graben has a simpler outcrop expression but both fault systems would be expected to have more complex fault geometries in the subsurface than used in the simplified model, enhancing the likelihood of further reservoir–reservoir juxtapositions and resultant cross-fault leak points in addition to areas identified in the simplified fault seal model.

Alternative fault seal algorithms that attempt to model the development of argillaceous smears within the faulted sequence include Clay Smear Potential (CSP; Bouvier et al., 1989; Fulljames et al., 1997) and Shale Smear Factor (SSF; Lindsay et al., 1993). The CSP algorithm is derived from studies on non-lithified clays with ductile smears while the SSF algorithm is based on lithified shales with abrasive-type smears. Both algorithms are reliant on defining smears resulting only from single argillaceous beds. For instances where more than one argillaceous bed is contributing to the smear, CSP and SSF represent only the bed with the greatest smear contribution. Local burial history curves from Nuccio and Condon (1996) indicate that faulting in the region would have occurred only in a lithified environment (i.e. abrasive-type smears), limiting the SSF algorithm as the only logical comparison to the SGR. Previous studies using the SSF (Lindsay et al., 1993; Takahashi, 2003) indicate that smears become discontinuous and cross-fault leakage can occur at values greater than 5–10, which would represent the blue, yellow and green areas in Fig. 9b. Compared to modelling results using the SGR (Fig. 9a), which predicts continuous smears forming from 20%, the SSF indicates most of the reservoir–reservoir juxtapositions in the Navajo and Wingate sandstones for both faults would most likely have cross-fault leakage due to non-development of continuous shale smears. Variations between the SGR and SSF in predicting continuous argillaceous smear development on the studied faults can probably be attributed to the SSF not incorporating argillaceous material from non-defined shale beds (cf. SGR) and not modelling compound smears (i.e. smears generated from multiple shale beds). Whether this suggests one smearing algorithm is better in predicting fault seal potential than the other is speculative as there is no definitive subsurface data available to confirm the cross-fault sealing capabilities of both studied faults. However, it does illustrate the variability in results depending on the smearing algorithm used and the need for good calibrations to known sealing and non-sealing faults in a region to define the best algorithm to use and its threshold values for sealing.

Based on these sensitivity analyses, the fault seal model generated for this study should be considered a best case scenario for seal potential, with a high probability of additional cross-fault leak points along both modelled faults. However, field evidence of fluid migration in the footwalls of both faults suggests a significant proportion of fluids are migrating parallel to the faults, a situation that cannot be modelled in current fault seal analysis workflows or is generally considered due to the probable multiple cross-fault leak points along both studied faults.

7. Discussion

7.1. Origin, timing and phase of fluid regimes

The CO_2-charged springs are a consequence of deep CO_2 mixing with one or more regional aquifers and eventually leaking to the surface in the footwalls of the studied faults. Previous studies on the origin of the CO_2 have varied with Shipton et al. (2004, 2005)

and Heath et al. (in press) suggesting a crustal source generated by clay–carbonate reactions in Palaeozoic source rocks such as the Paradox Formation. Wilkinson et al. (2008) argue for an additional mantle source from nearby igneous intrusions mixed with a younger crustal source mainly derived from diagenetic reactions in the shallower Navajo Sandstone. Regardless of its origin, all authors indicate that a proportion of the CO_2 has mixed with brines from as deep as the Paradox Formation, and that the resulting CO_2-rich brine has migrated vertically into the Navajo Sandstone before leaking to the surface in the study area. Dating of the travertines indicates this surface leakage and respective subsurface migration of CO_2 has been occurring for at least the last 100,000 years (Dockrill, 2006; Burnside et al., 2007, 2009). If a mantle source is invoked, CO_2 migration could date back to the Tertiary when the intrusives where emplaced in the region (Ross, 1998). Either way, CO_2 migration through this faulted stratigraphy has been a long-lived and pervasive event.

How the CO_2 interacts with the multiple aquifers and in what state it migrates through the faulted stratigraphy is also important as this indicates the likelihood that CO_2 could form significant subsurface accumulations or migrate straight through the faulted stratigraphy. If the CO_2 is undersaturated in the aquifers, it will migrate in solution. In this case migration is governed by one-phase flow and is controlled solely by rock permeability, limiting the effectiveness of seals to form absolute barriers and maintain significant subsurface fluid accumulations. Alternatively, if the CO_2 is oversaturated, it will migrate as a separate free phase; as supercritical CO_2 at depths generally greater than 800 m and as a gas at shallower depths (Herzog and Golomb, 2004). In two-phase flow, top or fault seals will be absolute until the capillary entry pressure of the seal rock is exceeded, and subsequent migration is controlled by rock permeability (e.g. Yielding et al., 1997; Bretan et al., 2003). Shipton et al. (2005) and Heath et al. (in press) assumed the CO_2 was sufficiently oversaturated to migrate as a free phase through the aquifers, forming multiple accumulations in the structural highs of the regional faulted aquifers analogous to migrating hydrocarbons. However, Wilkinson et al. (2008) used mass balance calculations to indicate that CO_2 is generally undersaturated in respect to the aquifers and that CO_2 migration is primarily in solution with a free phase only forming in fractures above the Navajo Sandstone. This is supported by Assayag et al. (2009) who used carbon isotopes to indicate CO_2 is undersaturated in the Navajo Sandstone aquifer. Based on the two later studies that considered aquifer geochemistry, CO_2 is likely to have migrated to the surface through multiple aquifers primarily in solution, with limited free-phase CO_2 accumulations forming in the regional aquifers. Regardless of whether CO_2 was a free phase or in solution, its migration pathway from source to surface was directed by zones of enhanced rock permeability associated with the studied faults.

The origin of the fluid(s) responsible for the bleaching of predominantly Mid-Jurassic sandstones in the footwalls of both faults is not clear, as more than one extra-formational fluid is capable of generating the bleached zones, including hydrocarbons, organic acids, methane and hydrogen sulphide (Surdam et al., 1993; Chan et al., 2000; Garden et al., 2001; Eichhubl et al., 2009). Previous studies of bleaching in the Paradox Basin have mainly attributed the bleaching fluid directly to hydrocarbons (Hansley, 1995; Chan et al., 2000; Garden et al., 2001; Beitler et al., 2003; Parry et al., 2004) or fluids directly associated with them (Eichhubl et al., 2009). One exception is Haszeldine et al. (2005) who suggest that water and $CO_2 + H_2S$ is responsible for the bleaching of the sandstone and that this fluid migrated along similar pathways to oil migration. The presence of a hydrocarbon seep and oil-stained sandstones in the Curtis and Morrison formations adjacent to the Little Grand Wash fault indicates that hydrocarbons may have caused the bleaching. However, the absence of hydrocarbons or associated features in the more extensively reduced northern footwall of the Salt Wash graben presents some doubt as to whether hydrocarbons were the bleaching fluid or if multiple fluids were involved. If hydrocarbons were responsible for the bleaching, the most likely hydrocarbon source would be organic-rich black shales from the Pennsylvanian Paradox Formation (Nuccio and Condon, 1996), though the Pennsylvanian Honaker Trail Formation, Permian Kaibab Limestone and Triassic Sinbad Limestone are also potential sources (Peterson, 1989; Huffman et al., 1996). The timing of hydrocarbon migration in the region has been confined to the early Tertiary along the Moab fault to the East (Garden et al., 2001) and to the Mid Tertiary in the Tar Sand Triangle to the South (Hansley, 1995; Huntoon et al., 1999). The presence of an active seep on the Little Grand Wash fault suggests that hydrocarbon migration continues to the present day, or that one or more subsequent pulses of hydrocarbons have charged the system from different sources. Migration of hydrocarbons from the Palaeozoic source through to the currently exposed Jurassic reservoirs with bleaching and beyond will be governed by two-phase flow.

Precipitation of the celestine veins ($SrSO_4$, Fig. 5j) require a Sr^{2+}-rich fluid to mix with a SO_4^{2-}-rich fluid or replace calcium sulphate minerals (i.e. gypsum or anhydrite) in-situ (Scholle et al., 1990). Precipitation of celestine probably results from Pennsylvanian-derived, Sr^{2+}-rich fluids rising through the stratigraphy and mixing with shallow SO_4^{2-}-rich meteoric waters or directly replacing gypsum precipitated in fractures. Analysis of meteoric waters erupting from geysers and springs along both faults by Heath et al. (in press) indicate the present-day waters are undersaturated in respect to sulphate. Thus, sulphate precipitation must predate the current fluid regime. The presence of reduction haloes around fractures infilled with sulphate suggests sulphate precipitation occurred during or after iron-oxide reduction as fracture pathways needed to be open to allow the migration of iron-reducing fluids. If hydrocarbons were responsible for iron-oxide reduction, sulphate precipitation commenced during or after the early Tertiary and ceased before start of the present-day meteoric conditions.

Considering the fluid-flow products that have been identified in the study area, it is apparent that varied fluid regimes (i.e. CO_2-rich brines, hydrocarbons, Sr-rich fluids) in differing fluid states (i.e. one- vs. two-phase flow) have utilised the same pathways to vertically migrate through this faulted stratigraphy over an extended period of time. This common migration pathway for multiple fluid regimes has been influenced by zones of enhanced permeability associated with the studied faults, which enable vertical migration through multiple cap rocks (i.e. Chinle, Moenkopi, Carmel and Morrison formations) and eventual leakage of fluids out of the system.

7.2. Structural controls on fluid migration

The trap geometry of the study area dictates that the studied faults play a primary role in the migration of fluids from source to reservoir and eventual leakage from the system. Multiple fluid regimes have utilised a common pathway parallel to the faults to migrate through the system. However, fault seal modelling of the Little Grand Wash fault suggests there should be multiple leak points along the juxtaposed reservoirs that permit across-fault flow, primarily due to throw partitioning associated with fault linkage and multiple fault strands. To comprehend why there is an inconsistency between the field and model-based approaches in identifying migration pathways, we need to appreciate what is encouraging fault-parallel flow in this faulted system. The two most likely options promoting vertical rather than across-fault flow are

1) incompetent cap rocks relative to the fault's sealing capabilities, or 2) enhanced fault-parallel permeability compared to the surrounding country rock enabling migration through overlying cap rocks.

Given that all the fluid regimes were likely sourced from at least as deep as the Paradox Formation, there are multiple formations that could act as cap rocks to inhibit vertical migration of fluids. The two most likely cap rock sequences are the Chinle and Moenkopi formations above the White Rim Sandstone and the Carmel Formation above the Navajo Sandstone. Combined, the Chinle and Moenkopi formations form a thick (>200 m), shale-rich sequence of fluvial and lacustrine deposits with minor marine incursions (Trimble and Doelling, 1978). Mercury injection measurements on the Moenkopi Formation by White et al. (2005) indicate that the unit could maintain a CO_2 column height of 100 m, suggesting the combined formations could provide a competent overlying cap rock sequence for any fluids migrating through the White Rim Sandstone. The Carmel Formation is a heterogeneous sabhka sequence of interbedded siliciclastics, carbonates and evaporates with the upper half containing over 50% anhydrite and gypsum (Trimble and Doelling, 1978). This unit is a proven seal for the nearby Farnham Dome field forming a competent cap rock above the Najavo Sandstone, which contains a 100 m CO_2 gas column. (Allis et al., 2001) Thus, cap rocks in the study area appear to be competent seals, with fault-parallel flow of multiple fluids more likely reliant on enhanced permeability associated with the faults rather than inadequate cap rocks.

To understand how enhanced permeability associated with the faults is promoting fault-parallel fluid flow, the specific migration pathways through the faulted stratigraphy needs to be identified. The migration pathways of these fluids can be determined through identifying the spatial distribution of their flow products in varied lithologies observed in the footwalls of both faults. In sand-rich formations (Entrada and Curtis) prevalent in the northern footwall of the Salt Wash graben, pervasive bleaching and numerous travertine deposits extend into the footwall around the fold axis of the Green River anticline. This distribution is consistent with fluids migrating up-dip and pooling at the crest of the faulted anticline. Distal to this area or in clay-rich stratigraphy, bleaching and travertine mineralisation is limited to the immediate footwall suggesting fracture networks developed in the damage zone of the fault play a role in the migration of fluids. This is readily evident in the clay-rich formations (Summerville and Morrison) of the Little Grand Wash fault footwall, where travertine mineralisation and bleaching is restricted to the immediate footwall, preferentially at structural complexities (i.e. relay zones and fault bends). Therefore, upon the migration of fluids to the crest of the faulted anticline, fluids vertically migrate through low-porosity, clay-rich units by utilising the fracture network developed in the damage zone of the fault. Fluid migration within the damage zone is concentrated in areas of structural complexity along the faults that include relay ramps, fault intersections and/or fault bends.

The localisation of fluid migration to structurally complex sections of the fault is a well documented phenomenon (Kerrich, 1986; Caine et al., 1996; Sibson, 1996; Curewitz and Karson, 1997; Gudmundsson et al., 2001; Gartrell et al., 2004; Eichhubl et al., 2009). Simple geometric models and field observations suggest fault terminations and or linkages between fault segments are domains of high fracture density and connectivity and are therefore likely to focus fluid flow (Curewitz and Karson, 1997). This was broadly demonstrated in this study with scanlines along the Little Grand Wash fault showing an increase in fracture density and range of orientations (and therefore fracture connectivity) surrounding a relay zone as opposed to a simpler section of the fault. Furthermore, distribution of fluid-flow products in shale-rich footwall sections of the studied faults were limited to areas of structural complexity involving relay ramps or fault bends. It is inferred these areas of structural complexity along the fault have enhanced permeability generated by the development of a fracture network due to complex stresses involved in fault linkage processes.

A significant proportion of fluids migrating through the study area are migrating parallel to the fault, utilising the damage zone fracture network of the fault with pathways focussed at areas of structural complexity with enhanced fracture connectivity. This study highlights the importance of a holistic approach when considering the seal integrity of a structural closure that emphasises the need for detailed mapping of structures to fully assess the risk of fault linkage creating unfavourable juxtapositions and flow pathways for vertical migration of fluids.

8. Conclusions

A protracted history of fault-related fluid flow is recorded within the footwalls of the Little Grand Wash fault and northern fault of the Salt Wash graben. Field evidence indicates hydrocarbons have and are migrating along the Little Grand Wash fault with regional studies indicating that migration commenced from the early Tertiary. Iron-oxide reduction in the footwalls of the Little Grand Wash fault and northern fault of the Salt Wash graben may be the result of this hydrocarbon migration, though the absence of hydrocarbons or hydrocarbon related features in the northern footwall of the Salt Wash graben suggests alternate or multiple fluid regimes could be responsible. Sporadic sulphate veins derived from SO_4^{2-} rich meteoric waters (gypsum) and rising Pennsylvanian brines (celestine) were precipitated during or after iron-oxide reduction and before the start of present-day meteoric water conditions. Precipitation of subsurface carbonate veins accompanied precipitation at the surface of travertine from present-day carbonate-rich meteoric waters. Our outcrop studies show that, where the footwall Upper Jurassic units are juxtaposed against shales in the hanging-wall, the fault core is dominated by low-permeability clay-rich gouge. Conversely, the surrounding damage zone is dominated by fractures both in the high-permeability reservoir units and in the low-permeability seal units. Furthermore, fracture orientation range and frequency are enhanced in zones of structural complexity improving fracture connectivity and providing possible pathways for fluids to migrate parallel to the fault. The presence of mineralisation and diagenesis within and bordering fractures in the footwall of both faults confirms that fault-parallel leakage occurred through the damage zone via the cap rocks. Modelling of the fault rocks at depth fails to predict such fault-parallel flow and underestimates the effect of complex fault architectures. Modelling of the effects of faults on fluid flow must include an appreciation of likely fault architectures and include an assessment of the relative permeabilities of the predicted fault seal, the cap rock and the faulted cap rock.

Acknowledgements

Funding for this work came from The Carbon Capture Project and the Trinity College Broad Curriculum Initiative. Midland Valley and Badley Geoscience generously provided 2DMove and 3DMove and Traptester software. John Walsh, Conrad Childs, Tom Manzocchi and Julian Strand provided constructive advice. Rick Allis provided a helpful review of an early version of this manuscript, and Peter Eichhubl, Chris Wibberley and an anonymous reviewer provided constructive reviews for this version. The team from Utah State University: Jim Evans, Jason Heath and Tony Williams provided assistance and constructive discussion in the field.

References

Allan, U.S., 1989. Model for hydrocarbon migration and entrapment within faulted structures. American Association of Petroleum Geologists Bulletin 73, 803–811.

Allis, R., White, S., Chidsey, T., Gwynn, W., Morgan, C. Adams, M., Moore, J., 2001. Natural CO_2 reservoirs on the colorado plateau and southern rocky mountains: candidates for CO_2 sequestration. In: Proceedings of the first national conference on Carbon sequestration, Washington DC, May 2001.

Allis, R., Bergfeld, D., Moore, J., McClure, K., Morgan, C., Chidsey, T., Heath, J., McPherson B., 2005. Implications of results from CO_2 flux surveys over known CO_2 systems for long-term monitoring. In: Proceedings of the Fourth Annual Conference on Carbon Sequestration and Sequestration, Virginia, May 2005.

Anderson, T.R.,, Fairley, J.P., 2008. Relating permeability to the structural setting of a fault-controlled hydrothermal system in southeast Oregon, USA. Journal of Geophysical Research 113, B05402. doi:10.1029/2007JB004962.

Assayag, N., Bickle, M., Kampman, N., Becker, J., 2009. Carbon isotopic constraints on CO_2 degassing in cold-water Geysers, Green River, Utah. Energy Procedia 1, 2361–2366.

Beitler, B., Chan, M.A., Parry, W.T., 2003. Bleaching of Jurassic Navajo sandstone on colorado plateau laramide highs; evidence of exhumed hydrocarbon supergiants? Geology 31, 1041–1044.

Bouvier, J.D., Kaars-Sijpesteijn, C.H., Kluesner, D.F., Onyejekwe, C.C., van der Pal, R.C., 1989. Three-dimensional seismic interpretation and fault sealing investigations, Nun River Field, Nigeria. American Association of Petroleum Geologists Bulletin 73, 1397–1414.

Breit, G.N., Meunier, J., 1990. Fluid inclusion, δ18O, and 87Sr/86Sr evidence for the origin of fault-controlled copper mineralization, Lisbon Valley, Utah, and Slick Rock District, Colorado. Economic Geology 85, 884–891.

Bretan, P., Yielding, G., Jones, H., 2003. Using calibrated shale gouge ratio to estimate hydrocarbon column heights. American Association of Petroleum Geologists Bulletin 87, 397–413.

Burnside, N., Shipton, Z.K., Ellam, R.M., 2007. Using spring deposits to track the evolution of fluid pathways through faults: little Grand Wash fault and Salt Wash graben, Utah, USA. Geological Society of America Abstracts with Programs 39, 240.

Burnside, N., Dockrill, B., Shipton, Z.K., Ellam, R.M., 2009. Dating and constraining leakage rates from a natural analogue for CO_2 storage: the Little Grand Wash and Salt Wash faults, Utah, USA. in: Faults and Top Seals: From Pore to Basin Scale, EAGE Conference volume extended abstract, Montpellier, France, 21–24 September 2009.

Caine, J.S., Evans, J.P., Forster, C.B., 1996. Fault zone architecture and permeability structure. Geology 24, 1025–1028.

Chan, M.A., Parry, W.T., Bowman, J.R., 2000. Diagenetic hematite and manganese oxides and fault-related fluid flow in Jurassic sandstones, Southeastern Utah. American Association of Petroleum Geologists Bulletin 84, 1281–1310.

Childs, C., Watterson, J., Walsh, J.J., 1996. A model for the structure and development of fault zones. Journal of the Geological Society of London 153, 337–340.

Childs, C., Walsh, J.J., Watterson, J., 1997. Complexity in fault zone structure and implications for fault seal prediction. In: Møller-Pedersen, P., Koestler, A.G. (Eds.), Hydrocarbon Seals - Importance for Exploration and Production. Norwegian Petroleum Society (NPF), Special Publication 7, 61–72.

Condon, S.M., 1997. Geology of the Pennsylvanian and Permian Cutler Group and Permian Kaibab limestone in the Paradox basin, southeastern Utah and southwestern Colorado. U.S. Geological Survey Bulletin 2000-P.

Curewitz, D., Karson, J.A., 1997. Structural settings of hydrothermal outflow; fracture permeability maintained by fault propagation and interaction. Journal of Volcanology and Geothermal Research 79, 149–168.

Dawers, N.H., Anders, M.H., 1995. Displacement-length scaling and fault linkage. Journal of Structural Geology 17, 607–614.

Dockrill, B., 2006. Understanding Leakage from a Fault-Sealed CO_2 Reservoir in East-Central Utah: A Natural Analogue Applicable to CO_2 Storage. Ph.D thesis, Trinity College Dublin.

Dockrill B., Kirschner, D.L., Shipton, Z.K., Internal structure and evolution of fault-related active and ancient travertine deposits in East-Central Utah, U.S.A. (in prep).

Doelling, H.H., 1994. Tufa deposits in western Grand County. Survey Notes – Utah Geological Survey 26, 8–10.

Doelling, H.H., Huntoon, P.W., Oviatt, C.G., 1988. Salt deformation in the Paradox region. Utah Geological and Mineral Survey Bulletin 122.

Doelling, H.H., 2001. Geologic map of the Moab and eastern part of the San Rafael Desert 30′ × 60′ quadrangles, Grand and Emery counties, Utah, and Mesa County, colorado. Utah Geological Survey, Map 180.

Doelling, H.H., 2002. Interim Geological Map of the San Rafael Desert 30′ × 60′ quadrangle, Grand and Emery County. Utah: Utah Geological Survey Map OFR-404.

Eichhubl, P., Davatzes, N.C., Becker, S.P., 2009. Structural and diagenetic Control of fluid migration and cementation along the Moab Fault, Utah. American Association of Petroleum Geologists Bulletin 93, 653–681.

Foxford, K.A., Walsh, J.J., Watterson, J., Garden, I.R., Guscott, S.C. and Burley, S.D.., 1998. Structure and content of the Moab fault zone, Utah, USA, and its implications for fault seal prediction. In Jones, G., Fisher, Q.J. and Knipe, R.J. (eds). Faulting, Fault Sealing and Fluid Flow in Hydrocarbon Reservoirs. Geological Society, London, Special Publications, 147, 87–103.

Fulljames, R.J., Zijerverld, L.J., Franssen, R.C.M.W., 1997. Fault seal processes: synthetic analysis of fault seals over geological and production time scales. In: Moller, P., Koestler, A.G. (Eds.), Hydrocarbon Seals: Importance for Exploration and Production. NPF Special Publication 7, 51–59.

Gartrell, A., Zhang, Y., Lisk, M., Dewhurst, D., 2004. Fault intersections as critical hydrocarbon leakage zones: integrated field study and numerical modelling of an example from the Timor Sea, Australia. Marine and Petroleum Geology 21, 1165–1179.

Garden, I.R., Guscott, S.C., Burley, S.D., Foxford, K.A., Walsh, J.J., Marshall, J., 2001. An exhumed palaeo-hydrocarbon migration fairway in a faulted carrier system, Entrada Sandstone of SE Utah, USA. Geofluids 1, 195–213.

Gibson, R.G., Bentham, P.A., 2003. Use of fault-seal analysis in understanding petroleum migration in a complexly faulted anticlinal trap, Columbus Basin, offshore Trinidad. American Association of Petroleum Geologists Bulletin 87, 465–478.

Gudmundsson, A., Berg, S.S., Lyslo, K.B., Skurtveit, E., 2001. Fracture networks and fluid transport in active fault zones. Journal of Structural Geology 23, 343–353.

Hansley, P.L., 1995. Diagenetic and burial history of the lower Permian white rim sandstone in the Tar sand triangle, Paradox basin, southeastern Utah. U.S. Geological Survey Bulletin 2000-I.

Haszeldine, R.S., Quinn, O., England, G., Shipton, Z.K., Evans, J.P., Heath, J., Crossey, L., Ballentine, C.J., 2005. Natural geochemical analogues for carbon dioxide storage and sequestration in deep geological porous reservoirsGas–Water Interactions. Special Issue of Oil & Gas Science and Technology (Revue de l'Inst Francais de Petrole 60, 1–12.

Heath, J.E., Lachmar, T.E., Evans, J.P., Kolesar, P.T., William, A.P., 2009. Hydrogeochemical characterization of leaking carbon dioxide-charged fault zones in east-central Utah, with implications for geologic carbon storage. In: McPherson, B., Sundquist, E. (Eds.), The Science and Technology of Carbon Sequestration. American Geophysical Union (AGU) Monograph 18, 147–158.

Herzog, H.J., Golomb, D., 2004. Carbon capture and storage from fossil fuel use. In: Cleveland, C.J. (Ed.), Encyclopedia of Energy. Elsevier Science Inc, New York, pp. 277–287.

Hesthammer, J., Fossen, H., 2000. Uncertainties associated with fault sealing analysis. Petroleum Geoscience 6, 37–45.

Hintze, J.F., 1993. Geological history of Utah. Brigham Young University Geology Studies, Special Publication 7.

Hood, J.W., Patterson, D.J., 1984. Bedrock aquifers in the northern San Rafael Swell area, Utah, with special emphasis on the Navajo sandstone. Utah Department of Natural Resources, Technical Publication 78.

Huffman, A.C., Lund, W.R., Godwin, L.H., 1996. Geology and resources of the Paradox basin. Utah Geological Association Publication 25.

Huntoon, J.E., Hansley, P.L., Naeser, N.D., 1999. The search for a source rock for the giant Tar Sand Triangle accumulation, southeastern Utah. American Association of Petroleum Geologists Bulletin 83, 467–495.

Kerrich, R., 1986. Fluid infiltration into fault zones; chemical, isotopic, and mechanical effects. Pure and Applied Geophysics 124, 225–268.

Knipe, R.J., 1997. Juxtaposition and seal diagrams to help analyze fault seals in hydrocarbon reservoirs. American Association of Petroleum Geologists Bulletin 81, 187–195.

Lindsay, N.G., Murphy, F.C., Walsh, J.J., Watterson, J., 1993. Outcrop studies of shale smears on fault surfaces. In: Flint, S.S., Bryant, I.D. (Eds.), The Geological Modelling of Hydrocarbon Reservoirs and Outcrop Analogues. Special Publication of the International Association of Sedimentologists 15, 113–123.

Lupton, C.T., 1914. Oil and gas near green River, Grand County, Utah. U.S. Geological Survey Bulletin 541-D, 115–133.

McKnight, E.T., 1940. Geology of the area between green and colorado rivers, Grand and San Juan counties, Utah. U.S. Geological Survey Bulletin 908.

Micklethwaite, S., 2009. Mechanisms of faulting and permeability enhancement during epithermal mineralisation: Cracow goldfield, Australia. Journal of Structural Geology 31, 288–300.

Midland Valley, 2004. 3DMove User Guide. Midland Valley, Glasgow, Scotland.

Moore, J., Adams, M., Allis, R., Lutz, S., Rauzi, S., 2005. Mineralogical and geochemical consequences of the long-term presence of CO_2 in natural reservoirs: an example from the Springerville–St. Johns Field, Arizona, and New Mexico, U.S.A. Chemical Geology 217, 365–385.

Morrison, S.J., Parry, W.T., 1986. Formation of carbonate-sulfate veins associated with copper ore deposits from saline basin brines, Lisbon Valley, Utah; fluid inclusion and isotopic evidence. Economic Geology 81, 1853–1866.

Nelson, S.T., Mayo, A.L., Gilfillan, S.M., Dutson, S.J., Harris, R.A., Shipton, Z.K., Tingey, D.G., 2009. Enhanced fracture permeability and accompanying fluid flow in the footwall of a normal fault: the Hurricane fault at Pah Tempe hot springs, Washington County, Utah. Geological Society of America Bulletin 121, 236–246.

Nicol, A., Watterson, J., Walsh, J.J., Childs, C., 1996. The shapes, major axis orientations and displacement patterns of fault surfaces. Journal of Structural Geology 18, 235–248.

Nuccio, V.F., Condon, S.M., 1996. Burial and thermal history of the Paradox basin, Utah and colorado, and the petroleum potential of the Middle Pennsylvanian Paradox formation. U.S. Geological Survey Bulletin 2000-O, 41.

Park, H.J., West, T.R., 2002. Sampling bias of discontinuity orientation caused by linear sampling technique. Engineering Geology 66, 99–110.

Parry, W.T., Chan, M.A., Beitler, B., 2004. Chemical bleaching indicates episodes of fluid flow in deformation bands in sandstone. American Association of Petroleum Geologists Bulletin 88, 175–191.

Peterson, P.R., 1973. Salt Wash field. Utah Geological Survey Oil and Gas Field Studies 4, 3.

Peterson, J.A., 1989. Geology and petroleum resources, Paradox basin Province. U.S. Geological Survey Open File Report, OF 88-0450-U, p. 69.

Pevear, D.R., Vrolijk, P.J., Longstaffe, F.J., 1997. Timing of Moab fault displacement and fluid movement integrated with burial history using radiogenic and stable isotopes. In: Hendry, J., Carey, P., Parnell, J., Ruffel, A., Worden, R. (Eds.), Geofluids II 1997 Extended Abstract Volume, pp. 42–45.

Ross, M.L., 1998. Geology of the Tertiary intrusive centers of the La Sal Mountains, Utah; influence of preexisting structural features on emplacement and morphology. U.S. Geological Survey Bulletin B-2158, 61–83.

Rotevatn, A., Hesthammer J., Fossen, H., Aas, T.E., and Howell J.., 2007. Are relay ramps conduits for fluid flow? Structural analysis of a relay ramp in Arches National Park, Utah. In Lonergan, L., Rawnsley, R.J.H. & Sanderson, D.J. eds. Fractured Reservoirs. Geological Society, London Special Publications, 270, 55–71.

Rowland, J.V., Sibson, R.H., 2004. Structural controls on hydrothermal flow in a segmented rift system, Taupo Volcanic Zone, New Zealand. Geofluids 4, 259–283.

Scholle, P.A., Stemmerik, L., Harpoth, O., 1990. Origin of major karst-associated celestite mineralization in Karstryggen, central East Greenland. Journal of Sedimentary Petrology 60, 397–410.

Shipton, Z.K., Evans, J.P., Kirschner, D., Kolesar, P.T., Williams, A.P., and Heath, J.., 2004. Analysis of CO_2 leakage through "low-permeability" faults from natural reservoirs in the Colorado Plateau, east-Central Utah. in, Baines, S.J. and R.H. Worden, eds. Geological Storage of Carbon Dioxide. Geological Society, London, Special Publications, 233, 3–59.

Shipton, Z.K, Evans, J.P., Dockrill, B., Heath, J., Williams, A.P., Kirschner, D., Kolesar, P.T., 2005. Natural leaking CO_2-charged systems as analogues for failed geologic storage reservoirs. In, Benson, S.M., Oldenburg C., Hoversten M., S. Imbus, eds., Carbon Dioxide Capture for Storage in Deep Geological Formations- Results from the CO_2 Capture Project, pp. 699–712.

Sibson, R.H., 1996. Structural permeability of fluid-driven fault-fracture meshes. Journal of Structural Geology 18, 1031–1042.

Sperrevik, S., Faerseth, R.B., Gabrielsen, R.H., 2000. Experiments on clay smear formation along faults. Petroleum Geoscience 6, 113–123.

Surdam, R.C., Jiao, Z.S., MacGowan, D.B., 1993. Redox reactions involving hydrocarbons and mineral oxidants; a mechanism for significant porosity enhancement in sandstones. American Association of Petroleum Geologists Bulletin 77, 1509–1518.

Takahashi, M., 2003. Permeability change during experimental fault smearing. Journal of Geophysical Research 108 (B5), 2235,. doi:10.1029/2002JB001984.

Trimble, L.M., Doelling, H.H., 1978. Geology and uranium-vanadium deposits of the San Rafael River mining area, Emery County, Utah. Utah Geological and Mineral Survey Bulletin 113, 112.

Vrolijk, P., Myers, R., Sweet, M.L., Shipton, Z.K., Dockrill, B., Evans, J.P., Heath, J., Williams, A.P., 2005. Anatomy of reservoir-scale normal faults in central Utah: stratigraphic controls and implications for fault zone evolution and fluid flow. GSA Field Guide 6: Interior Western United States 6, 261–282.

White, S.P., Allis, R.G., Moore, J., Chidsey, T., Morgan, C., Gwynn, W., Adams, M., 2005. Simulation of reactive transport of injected CO_2 on the Colorado Plateau, Utah, USA. Chemical Geology 217, 387–405.

Wilkinson, M., Gilfillan, S.M.V., Haszeldine, R.S., Ballentine, C.J., 2008. Plumbing the depths – testing natural tracers of subsurface CO_2 origin and migration, Utah, USA. In: Grobe, M., Pashin, J.C., Dodge, R.L. (Eds.), Carbon Dioxide Sequestration in Geological Media — State of the Science. AAPG Studies 59, 1–16.

Williams, P.L., 1964. Geology, structure, and uranium deposits of the Moab Quadrangle, Colorado and Utah. U.S. Geological Survey Miscellaneous Investigation Series, Map I-360.

Williams, A.P., 2005. Structural Analysis of the Little Grand Wash and Salt Wash faults to Investigate the Leakage of CO2 from a Natural Reservoir. M.S. thesis, Utah State Univ.

Yielding, G., 2002. Shale Gouge ratio: calibration by geohistory. In: Koestler, A.G., Hunsdale, R. (Eds.), Hydrocarbon Seal Quantification. NPF Special Publication 11, 1–15.

Yielding, G., Freeman, B., Needham, D.T., 1997. Quantitative fault seal prediction. American Association of Petroleum Geologists Bulletin 81, 897–917.